ORIGINAL ARTICLE: REPRODUCTIVE SCIENCE

Metabolic imaging of human cumulus cells reveals associations among metabolic profiles of cumulus cells, patient clinical factors, and oocyte maturity

Marta Venturas, M.Sc.,[a,b] Xingbo Yang, Ph.D.,[a] Kishlay Kumar, Ph.D.,[c] Dagan Wells, Ph.D.,[c,d] Catherine Racowsky, Ph.D.,[e,f] and Daniel J. Needleman, Ph.D.[a,g]

[a] Molecular and Cellular Biology and School of Engineering and Applied Sciences, Harvard University, Cambridge, Massachusetts; [b] Department de Biologia Cellular, Fisiologia i Immunologia, Universitat Autònoma de Barcelona, Cerdanyola, Spain; [c] Nuffield Department of Women's and Reproductive Health, John Radcliffe Hospital, Oxford University, Oxford, United Kingdom; [d] Juno Genetics, Oxford Science Park, Oxford, United Kingdom; [e] Brigham and Women's Hospital and Harvard Medical School, Boston, Massachusetts; [f] Department of Obstetrics and Gynecology and Reproductive Medicine, Hospital Foch, Suresnes, France; and [g] Center for Computational Biology, Flatiron Institute, New York, New York

Objective: To determine whether fluorescence lifetime imaging microscopy (FLIM) detects differences in metabolic state among cumulus cell samples and whether their metabolic state is associated with patient age, body mass index (BMI), and antimüllerian hormone (AMH) level and maturity of the oocyte.
Design: Prospective observational study.
Setting: Academic laboratory.
Patient(s): Cumulus cell (CC) clusters from cumulus-oocyte complexes were collected from patients undergoing assisted reproductive technology treatment after oocyte retrieval and vitrified.
Intervention(s): Cumulus cell metabolism was assessed using FLIM to measure autofluorescence of nicotinamide adenine (phosphate) dinucleotide and flavine adenine dinucleotide, endogenous coenzymes essential for cellular respiration and glycolysis. Patient age, BMI, and AMH level and the maturity of the corresponding oocytes were recorded.
Main Outcome Measure(s): Quantitative information from FLIM was obtained regarding metabolite concentrations from fluorescence intensity and metabolite enzyme engagement from fluorescence lifetimes. Associations were investigated between each FLIM parameter and oocyte maturity and patient age, BMI, and AMH. Variance between CC clusters within and between patients was determined.
Result(s): Of 619 CC clusters from 193 patients, 90 were associated with immature oocytes and 505 with metaphase II oocytes. FLIM enabled quantitative measurements of the metabolic state of CC clusters. These parameters were significantly correlated with patient age and AMH independently, but not with BMI. Cumulus cell nicotinamide adenine (phosphate) dinucleotide FLIM parameters and redox ratio were significantly associated with maturity of the enclosed oocyte.
Conclusion(s): FLIM detects variations in the metabolic state of CCs, showing a greater variance among clusters from each patient than between patients. Fluorescence lifetime imaging microscopy can detect CC metabolic associations with patient age and AMH and variations between mature and immature oocytes, suggesting the potential utility of this technique to help identify superior oocytes. (Fertil Steril® 2021;■:■–■. ©2021 by American Society for Reproductive Medicine.)
Key Words: Cumulus cells, cumulus-oocyte complexes, fluorescence lifetime imaging microscopy, human oocytes, maturity, metabolism

DIALOG: You can discuss this article with its authors and other readers at https://www.fertstertdialog.com/posts/32893

Received April 15, 2021; revised July 27, 2021; accepted July 29, 2021.
M.V. has nothing to disclose. X.Y. has nothing to disclose. K.K. has nothing to disclose. D.W. reports receiving a grant from the National Institutes of Health for the submitted work. C.R. heports receiving a grant from the National Institutes of Health for the submitted work. D.J.N. reports receiving a grant from the National Institutes of Health for the submitted work.
Supported by National Institutes of Health grant NIH R01HD092550-03 (to C.R., D.W., and D.J.N.).
Reprint requests: Marta Venturas, M.Sc., Molecular and Cellular Biology and School of Engineering and Applied Sciences, Harvard University, Cambridge, MA 02138 (E-mail: marta_venturas@fas.harvard.edu).

Fertility and Sterility® Vol. ■, No. ■, ■ 2021 0015-0282/$36.00

https://doi.org/10.1016/j.fertnstert.2021.07.1204

Extensive evidence supports the role of bidirectional crosstalk between the oocyte and its surrounding cumulus mass for successful oocyte development (1, 2). Oocyte growth is dependent on metabolic cooperation between the oocyte and its cumulus cells (CCs), which is facilitated by the exchange of molecules through gap junctions and paracrine signals (3, 4). This interaction is bidirectional: CCs provide growth factors, lipids, and metabolites for oocyte maturation and development (5–7), and oocyte-secreted factors enable differentiation and mucification of CCs (8, 9).

Oocyte developmental potential depends on oocyte quality (7), which in turn, is reflected in nuclear and cytoplasmic maturity, both of which are essential for successful fertilization and embryo development (10). In addition, CCs help maintain the oocyte in meiotic arrest at prophase I (1). This communication is essential for the resumption of meiosis in response to the luteinizing hormone surge (11). Conversely, meiotic status can influence the metabolism not only of the oocyte, but also of the surrounding cumulus mass. Pyruvate consumption by cumulus-oocyte complexes (COCs) has been positively associated with oocyte nuclear maturation (8, 12). Moreover, mitochondrial dysfunction and mitochondrial DNA (mtDNA) copy number of CCs might be directly related to oocyte maturity (13–15).

Because of the intimate interactions between the oocyte and its surrounding CC mass, measurements of the metabolic state of CCs are a promising means to determine the developmental competence of the associated oocyte (16–19). Because cumulus masses are routinely removed for intracytoplasmic sperm injection and are frequently trimmed before conventional insemination, these otherwise discarded cells have the potential for use in a noninvasive assay of oocyte developmental competence (20–25). However, reliable biomarkers in CCs have yet to be identified (23).

A number of recent studies have focused on measurements of mtDNA in CCs, the results of which have been inconclusive (17, 18, 26). Some studies found that mtDNA copy number does not seem to be associated with oocyte maturity or fertilization (18), whereas other studies observed a correlation with oocyte fate (14, 15). Other studies have used mitochondrial dyes (13, 27) to study mitochondrial activity in CCs. Establishing quantitative tools to measure the metabolic state of single cumulus complexes could be helpful for developing an improved understanding of the metabolic relationship between CCs and the enclosed oocyte and might enable noninvasive approaches to evaluate oocyte maturity and overall quality.

Nicotinamide adenine dinucleotide (NADH), nicotinamide adenine phosphate dinucleotide (NADPH), and flavine adenine dinucleotide (FAD+) are central metabolic coenzymes that are naturally fluorescent (28). These molecules are electron carriers that have essential roles in metabolic pathways, such as the electron transport chain and glycolysis, and therefore they are ideal biomarkers of cellular metabolic state (29, 30). The fluorescence spectra of NADH and NADPH are almost indistinguishable (31), and therefore the combined fluorescence of NADH and NADPH is often referred to as the NAD(P)H signal. Fluorescence lifetime imaging microscopy (FLIM) of NAD(P)H and FAD+ provides a means to measure the fluorescence intensity and fluorescence lifetime of these molecules. The fluorescence intensity is related to the concentrations of the coenzymes, whereas the fluorescence lifetime depends on the local environment of the coenzyme, varying drastically according to whether it is bound to an enzyme or free (32).

In the present study, we used metabolic imaging by FLIM to measure the metabolic state of CCs in vitro. We evaluated the sensitivity of this noninvasive metabolic imaging to investigate the associations among clinically relevant patient factors, such as maternal age, body mass index (BMI), and antimüllerian hormone (AMH) level, and the metabolic state of the cumulus masses. Finally, we explored the extent to which quantitative measures of the metabolic state of CC clusters are associated with the maturity of the oocyte they enclose.

MATERIALS AND METHODS

Study Design

CC clusters were donated for research under consent by patients undergoing assisted reproductive technology treatment after institutional review board approval of the study protocol by Partners Healthcare institutional review board (Partners institutional review board no. 2014P000874).

After collection, vitrification, and subsequent thawing, the metabolic state of each CC cluster was assessed using metabolic imaging by FLIM. Patient age, BMI, and AMH level within 6 months after treatment, follicle-stimulating hormone and luteinizing hormone levels, the number of oocytes retrieved, and the percentage of mature oocytes (number of mature oocytes/total number of oocytes retrieved) were recorded. The meiotic status of each oocyte was retrospectively tied to its corresponding CC cluster.

Sample Preparation

Cumulus-oocyte complexes were retrieved with the use of standard clinical protocols after ovarian stimulation and ovulatory trigger, isolated, set up in individual drops of 25 μL of culture medium (Global Total, Life Global Group, Cooper Surgical, Guilford, Connecticut) overlaid with oil (Vitrolife Ovoil, Göteborg, Sweden), and incubated for 1 to 4 hours. The CC masses of each oocyte were trimmed, and the trimmed CCs were rinsed and vitrified following the Irvine vitrification protocol (90133-SO-Vit Kit-Freeze, FUJIFILM Irvine Scientific, USA). Each CC mass was then thawed, following the Irvine thawing protocol (90137-SO-Vit Kit-Thaw, FUJIFILM Irvine Scientific), and their hyaluronan matrix was disaggregated after exposure to hyaluronidase (80 IU/mL of hyaluronidase, FUJIFILM Irvine Scientific). The disaggregated CCs were centrifuged, and the pellet, which consisted of a cluster of CCs, was collected. The clusters were then placed in 5-μL droplets of culture medium covered with oil in a glass-bottomed dish (MatTek P35G-0.170-14-C) designed for imaging. The CC clusters were imaged in an on-stage incubation system (Ibidi, Martinsried, Germany) to maintain culture environmental conditions of 37°C and 5% CO_2, 5% O_2, balanced with N_2.

Staining Protocols

For TMRM (tetramethylrhodamine, methyl ester) experiments, the CC clusters were incubated with 5 nM of TMRM (Thermo Fisher, USA) for 10 minutes. For DNA staining experiments, the CCs were stained with 1:400 of Syto 9 (Thermo Fisher) for 60 minutes. The samples were then washed three times through culture media (Global Total) and transferred to a glass-bottomed dish for imaging.

Metabolic Imaging by FLIM

FLIM measurements were performed with a Nikon Eclipse Ti microscope using two-photon excitation from a Ti:Sapphire pulsed laser (Mai-Tai, Spectral-Physics) with an 80-MHz repetition rate and 70-fs pulse width, a Galvano scanner (DCS-120, Becker and Hickl, Germany), a TCSPC module (SPC-150, Becker and Hickl), and a hybrid single-photon counting detector (HPM-100-40, Becker and Hickl). The wavelength of excitation was set to 750 nm for NAD(P)H and 890 nm for FAD+, with powers measured at the objective of 3 mW for NAD(P)H and 16.8 mW for FAD+. Optical bandpass filters were positioned in a filter wheel in front of the detector at 460/50 nm for NAD(P)H and 550/88 nm for FAD+, and a 650-nm short pass filter (Chroma Technologies) was mounted on the detector. Imaging was performed with a ×40 Nikon objective with 1.25 numerical aperture (CFI Apo 40 × WI, numerical aperture 1.25, Nikon). Each NAD(P)H and FAD+ FLIM image was acquired within 60 seconds of integration time. Objective piezo stage (P-725, Physik Instruments) and motorized stage (ProScan II, Prior Scientific) were used to perform multidimensional acquisition. Ten images were acquired per cumulus cluster varying the x, y, and z axis. All the electronics were controlled by SPCM software (Becker and Hickl) and custom LabVIEW software.

Data Analysis

The data were analyzed by customized MATLAB (version R2019b, MathWorks) code. NAD(P)H and FAD+ FLIM intensity images were subjected to an intensity-based threshold to classify pixels as being in cells or background. For each cell segment, the photon arrival time histogram was modeled as a biexponential decay:

$$P(t) = A\left[(1-F) * e^{-t/\tau_1} + F * e^{-t/\tau_1}\right] + B \quad (1)$$

where A is a normalization factor, B is the background, τ_1 is the short lifetime, τ_2 is the long lifetime, and F is the fraction of the molecule with a long lifetime (the fraction engaged for NAD(P)H and unengaged with enzymes for FAD+). This function was convolved with a measured instrument response function, and a least-square fit was used to determine the parameters. The fluorescence intensity was calculated for each CC cluster as the number of photons divided by the area of the cluster. Thus, a single FLIM measurement produced nine parameters, four for NAD(P)H, four for FAD+, and one redox ratio (NAD(P)H fluorescence intensity/FAD+ fluorescence intensity) to characterize the metabolic state of the CC clusters.

Statistical Analysis

All statistical tests were performed with Stata Statistical Software (version 16.0, LLC Stata Corp, Texas) and R Studio (Version 1.3.959, R Foundation for Statistical Computing, Vienna, Austria). Our data were structured hierarchically, with 1 to 10 images for each cluster (i) and one to four clusters (j) per patient (k). We thus used multilevel models, on the standardized FLIM parameters ($\frac{x-mean(x)}{sd}$), to analyze these structured data. Data points that lay 40% above or below the mean were considered outliers and removed from the analysis. We incorporated additional predictors (age, BMI, AMH level, and oocyte maturity) for certain analyses, resulting in the multilevel model

$$FLIMparam_{ijk} = \beta_0 + \beta_1 * Patient\ Factor + c_{0,k} + b_{0,jk} + e_{ijk}$$

where β_0 corresponds to the intercept; β_1 is the slope; *Patient Factor* is age, BMI, AMH level, or oocyte maturity (if considered); $c_{0,k}$ is the patient-level random error; $b_{0,jk}$ is the cluster-level random error; and e_{ijk} is the image-level random error (33). This modeling encodes information on the variance associated with each level: patient, CC clusters within patients, and images within CC cluster. To correct for multiple comparisons, we used the Benjamini-Hochberg false discovery rate (FDR) at a q value of .05. FDR P values $<.05$ were considered to indicate statistical significance.

RESULTS

NAD(P)H Autofluorescence of CCs Predominantly Originates from the Mitochondria

We first sought to explore the subcellular localization of NAD(P)H and FAD+ autofluorescence. After the dissociated CCs were centrifuged from a cluster, the resulting pellet was moved to an on-stage incubation system and imaged for NAD(P)H and FAD+ autofluorescence (Fig. 1A and B, respectively) with FLIM. Each acquired image was 220 × 220 μm, containing tens to hundreds of CCs (Fig. 1A and B, *left panels*), but represented only a small region of an entire CC pellet. To quantitatively analyze the CC metabolic state in the imaged region, we used an intensity-based threshold to create masks (Fig. 1A and B, *right panels*). We grouped all photons from each of the masked regions to create histograms of the fluorescence decay of NAD(P)H (Fig. 1C, *upper*, blue) and FAD+ (Fig. 1C, *lower*, green). We then fit these histograms using two-exponential decay models (equation 1) (Fig. 1C, black lines), thereby obtaining a total of six parameters: short and long lifetimes and the fraction of engaged molecules, for both NAD(P)H and FAD+. In addition, we computed NAD(P)H intensity, FAD+ intensity, and redox ratio, providing a total of nine quantitative metabolic parameters for each cluster.

Whereas FAD+ is highly enriched in the mitochondria (29), NADH and NADPH participate in different pathways in the mitochondria, the nucleus, and the cytoplasm (31, 32, 34). To better understand the source of the NAD(P)H signal in CCs, we compared NAD(P)H images with images using dyes for either mitochondria or DNA. We first stained a cumulus mass with TMRM, a dye known to localize to active

FIGURE 1

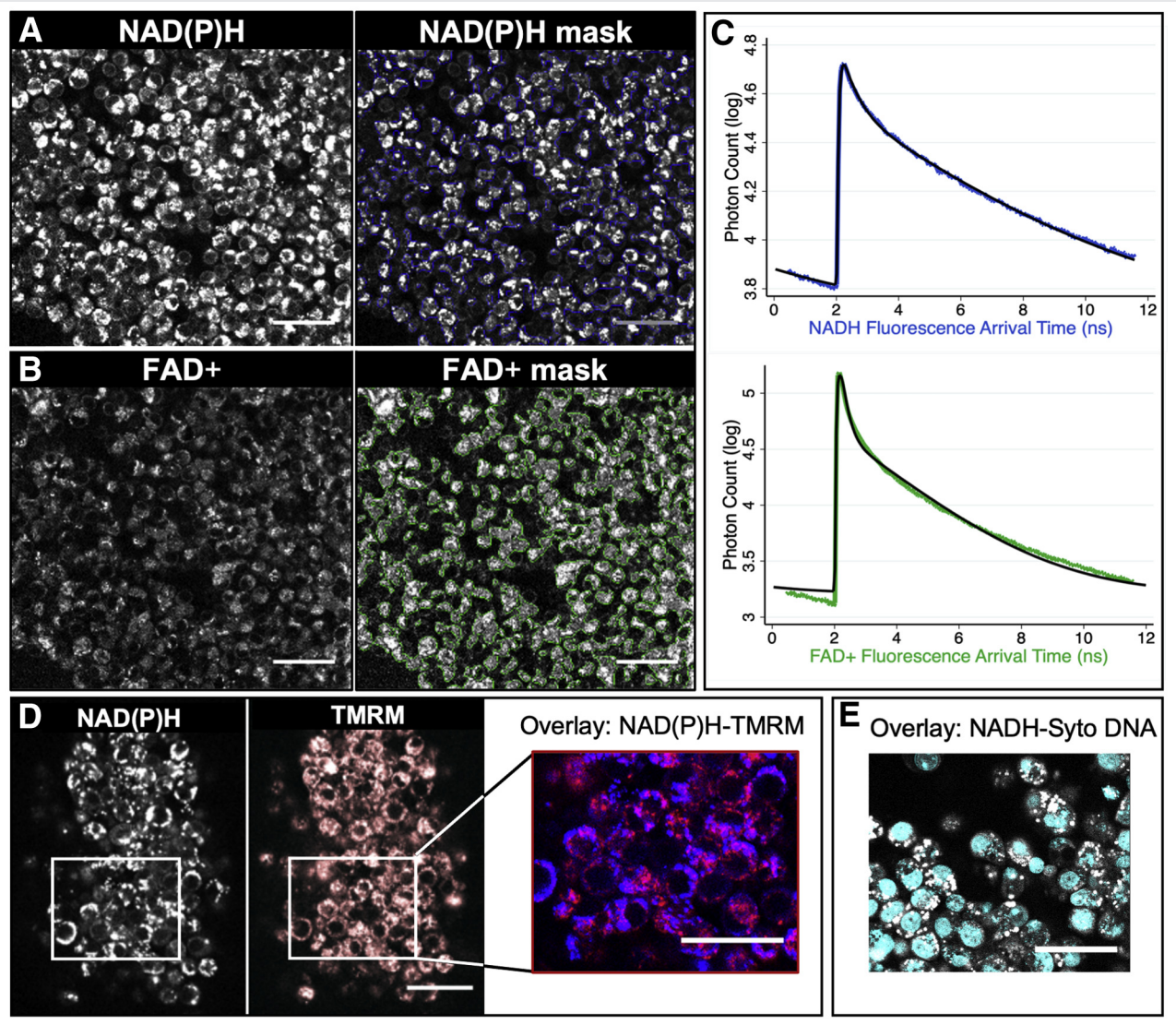

FLIM imaging of CCs. FLIM imaging of the autofluorescence of NAD(P)H (**A**) of a CC mass and FAD+ (**B**). An intensity-based thresholding algorithm was used to create masks of CCs to integrate the fluorescence signal of NAD(P)H or FAD+ (*right panels*). All photon arrival times from that mask were combined to create a fluorescence decay curve for each fluorophore (NAD(P)H in blue, **C** *top* and FAD+ in green, **C** *bottom*). These curves were fit to two-exponential models (**C**, black curves). This approach provides nine quantitative parameters for characterizing the metabolic state of CCs: fluorescence intensity, long and short lifetime, and the fraction engaged to enzyme for molecules NAD(P)H and FAD+ and the redox ratio. (**D**) NAD(P)H autofluorescence (*left*) image showing colocalization with mitochondria dye TMRM image (in red, *overlay* in purple). (E) *Overlay* image of NAD(P)H autofluorescence in gray and DNA dye Syto in cyan. Bar = 40 μm. CC = cumulus cell; FAD+ = flavine adenine dinucleotide; FLIM = fluorescence lifetime imaging microscopy; NAD(P)H = nicotinamide adenine (phosphate) dinucleotide; TMRM = tetramethylrhodamine methyl ester.

Venturas. Metabolic imaging of human cumulus cells. Fertil Steril 2021.

mitochondria (Fig. 1C). We segmented the mitochondria from the TMRM images using machine-learning-based segmentation software (Illastik, version 1.0) (35), and by comparing the overlap of the segmented TMRM and NAD(P)H images, we determined that 73% ± 5% of NAD(P)H photons came from the mitochondria. We next stained the cumulus mass with Syto 9, a DNA dye (Fig. 1E), and by comparing the overlap with the NAD(P)H signal, we found that 16% ± 1% of the NAD(P)H photons came from the nucleus. Hence, the remaining photons came from the cytoplasm. Thus, although the acquired NAD(P)H signal had contributions from all compartments, the majority of the signal came from the mitochondria.

CC Processing for FLIM Analysis

We next explored the extent to which variations in sample preparation procedures impacted the results of FLIM measurements of CC clusters. Cumulus cells that were imaged fresh

gave FLIM parameters that were indistinguishable from those of CCs that were first vitrified and then thawed (Supplemental Fig. 1, available online). Because vitrified samples are more convenient to work with than fresh samples, we opted to vitrify CCs in subsequent experiments. We next tested the impact of hyaluronidase on the FLIM parameters of CCs. The fraction engaged and lifetimes of CCs that were not exposed to hyaluronidase, and thus maintained their hyaluronan matrix, were indistinguishable from those of CCs that were dispersed with hyaluronidase (Supplemental Fig. 2). However, CCs not exposed to hyaluronidase did give significantly different intensities and redox ratios, which were likely caused by difficulties in successfully segmenting these far less dense cells. Therefore, we used vitrified CCs exposed to hyaluronidase in subsequent experiments.

We then explored how the location of the CCs within a cumulus cluster impacted the results of FLIM measurements. Fluorescence lifetime imaging microscopy parameters of CCs that were trimmed from closer to the oocyte did not show significant differences from those of CCs that were trimmed further from the oocyte (Supplemental Fig. 3). Because damage to the oocyte is less likely the further the CCs are trimmed from the oocyte, we trimmed the CCs further from the oocyte in all subsequent sample collections. Taken together, these experiments led us to use CCs trimmed further from the oocytes, which were vitrified and then exposed to hyaluronidase before imaging.

The Metabolic Variance Between CC Clusters Exceeds the Variance Between Patients and Between Images

A total of 619 CC samples were collected from 193 patients, 90 of which were associated with immature oocytes, 58 at the germinal vesicle stage and 32 at metaphase I; 505 were associated with mature oocytes, and 24 were associated with either degenerated or abnormal oocytes. We acquired from 8 to 10 nonoverlapping FLIM images at different locations throughout each CC pellet (Fig. 2A). We used a multilevel model (33, 36) to analyze these hierarchically organized data and decomposed the variance in the FLIM parameters into three levels: variance associated with differences between patients, variance associated with differences between CC clusters from the same patient, and variance associated with differences between individual images from the same CC cluster. For all FLIM parameters, the variance associated with differences between CC clusters from one patient was substantially larger than the variance associated with differences between individual images and the variance associated with differences between patients (Fig. 2B). The large variance in FLIM parameters associated with CC clusters indicates that different clusters from the same patient have significantly different metabolic states. The small variance in FLIM parameters associated with differences between individual images suggests a relative homogeneity of metabolic state within a CC cluster and demonstrates the high robustness and reproducibility of these measurements. Although it is small, the variance in FLIM parameters associated with differences between patients indicates that patient-specific factors impact the metabolism of their CCs.

CC Metabolic Parameters Are Associated with Maternal Clinical Factors

We next explored the extent to which maternal age, AMH level, and BMI independently account for the variance in FLIM parameters associated with differences between patients. These factors varied greatly across the 193 patients we studied. Maternal age ranged from 23.5 to 45 years, with a mean of 36.7 years; 58.0% of the patients were less or equal than 38 years old and 42.0% were more than 38 years old. AMH level ranged from 0.1 to 12 ng/mL, with a mean of 2.9 ng/mL. BMI ranged from 17.8 to 49.5 kg/m^2, with a mean of 26.7 kg/m^2; 49.8% of the patients had a BMI lower or equal than 24.9 kg/m^2, 38.8% had a BMI between 25 and 29.9 kg/m^2, and 11.4% had a BMI greater or equal than 30 kg/m^2. Plotting FLIM parameters vs. maternal age and AMH level revealed apparent associations (Fig. 3A and B, respectively). Incorporating these patient factors into the multilevel model allowed us to determine that maternal age was significantly correlated with NAD(P)H irradiance, fraction engaged, and long lifetime and with FAD+ fraction engaged and short lifetime, whereas AMH level was significantly correlated with NAD(P)H irradiance, fraction engaged, and both short and long lifetime and with FAD+ irradiance and short lifetime (Fig. 3D). The correlations with maternal age remained after controlling for AMH level, and the correlations with AMH level remained after controlling for maternal age. In contrast, we found no significant correlations between any FLIM parameters and maternal BMI (Fig. 3C and D) or when the BMI was stratified by the three groups. However, the percentage of the variance in CC FLIM measurements between patients was not entirely explained by maternal age and AMH level, suggesting that other patient-specific factors impact the metabolic state of their CC clusters (Fig. 3D). In consistency with this, we also found that the levels of both follicle-stimulating hormone and luteinizing hormone administered were significantly correlated with FLIM parameters (FDR $P<.05$). However, these associations were dependent on both maternal age and AMH level, suggesting that the amount of gonadotropin administered might not directly cause changes in FLIM parameters. Further studies will be necessary to disentangle the interactions between patient-specific factors that impact CC FLIM parameters.

CC FLIM Parameters Are Associated with the Maturity of the Enclosed Oocyte

We next sought to determine if the metabolic state of CC clusters was correlated with the maturity of the oocyte with which they were associated. The percentage of mature oocytes (of total oocytes retrieved) from a patient was not associated with maternal age ($P=.20$), BMI ($P=1.0$), AMH level ($P=.74$), or the total number of oocytes retrieved from that patient ($P=.69$) (Fig. 3A and B). Comparison of CC FLIM parameters from mature oocytes with those from immature oocytes revealed several interesting contrasts: NAD(P)H irradiance

FIGURE 2

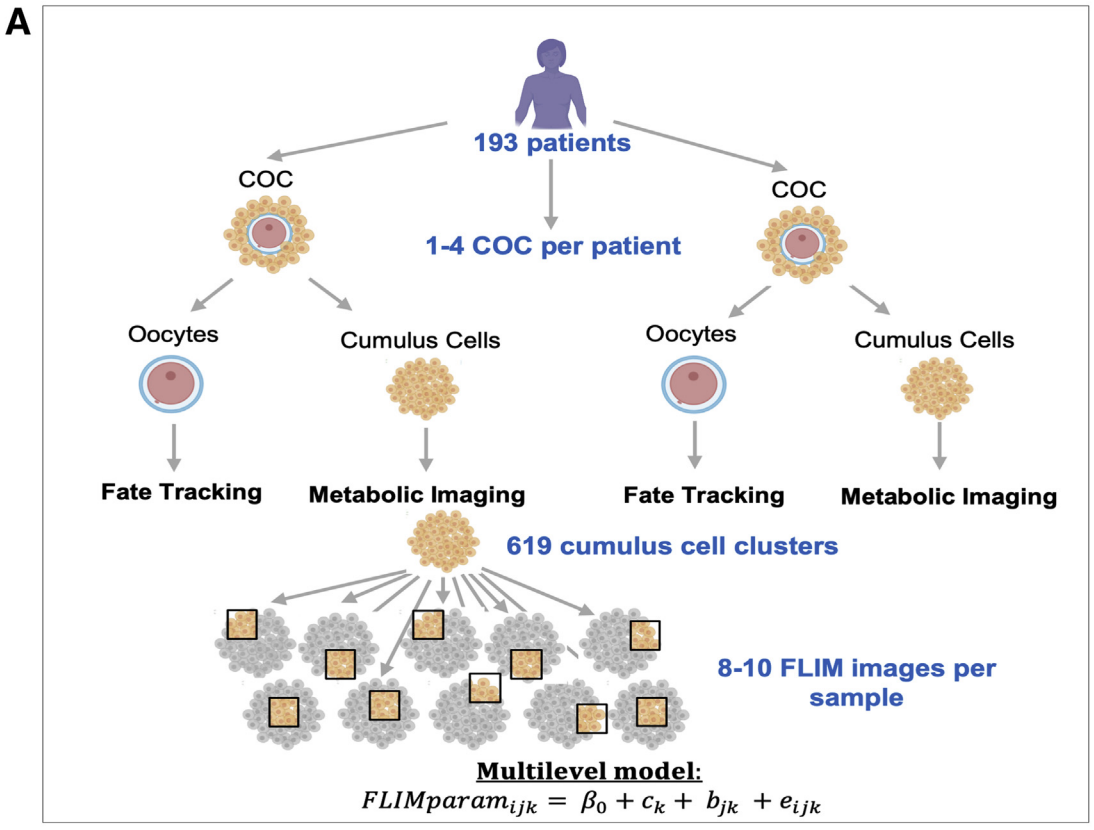

B

Level	NAD(P)H irradiance	NAD(P)H Fraction Engaged	NAD(P)H Long Lifetime	NAD(P)H Short Lifetime	FAD+ irradiance	FAD+ Fraction Engaged	FAD+ Long Lifetime	FAD+ Short Lifetime	Redox Ratio
$Var(c_k)$	0.30	0.23	0.27	0.18	0.29	0.15	0.47	0.19	0.21
$Var(b_{jk})$	0.59	0.67	0.63	0.72	0.55	0.74	0.83	0.69	0.84
$Var(e_{ijk})$	0.10	0.13	0.19	0.30	0.07	0.15	0.13	0.15	0.08

Metabolic variance between patients, between CCs, and between images. **(A)** Diagram of the experimental design of this study. From one to four COCs were collected per patient. Cumulus cell masses were trimmed from the COCs and imaged using metabolic imaging. The fate of the corresponding oocyte was monitored. From 8 to 10 FLIM metabolic images at different locations throughout the cluster were taken for each cumulus cluster. A multilevel model was applied to analyze these structured data. (**B**) The multilevel model encodes information on the variance of each FLIM parameter between patients, between CC clusters from the same patient, and between images from the same CC cluster. Numbers in the table correspond to the variance of each FLIM parameter associated with each level: patients, CC clusters, and images. CC = cumulus cluster; COC = cumulus-oocyte complex; FAD+ = flavine adenine dinucleotide; FLIM = fluorescence lifetime imaging microscopy; NAD(P)H = nicotinamide adenine (phosphate) dinucleotide.

Venturas. Metabolic imaging of human cumulus cells. Fertil Steril 2021.

(FDR P=.02), fraction engaged (FDR $P<1 \times 10^{-5}$), long lifetime (FDR $P<1 \times 10^{-5}$), and redox ratio (FDR P=.02) significantly differed between mature and immature oocytes (Fig. 4C–E). These significant differences remained after controlling for maternal age and AMH level. Plotting these three FLIM parameters for each CC cluster on a three-dimensional graph revealed that whereas the distributions significantly differed between CCs from mature and immature oocytes, there was also substantial overlap between these two populations (Fig. 4E, blue, immature; yellow, mature; gray, support vector machine-generated hyperplane that best separates the two populations).

DISCUSSION

Metabolic interconnections between CCs and oocytes are essential for cumulus mass expansion and maturation and development of oocytes (25). Mitochondrial dysfunction in

FIGURE 3

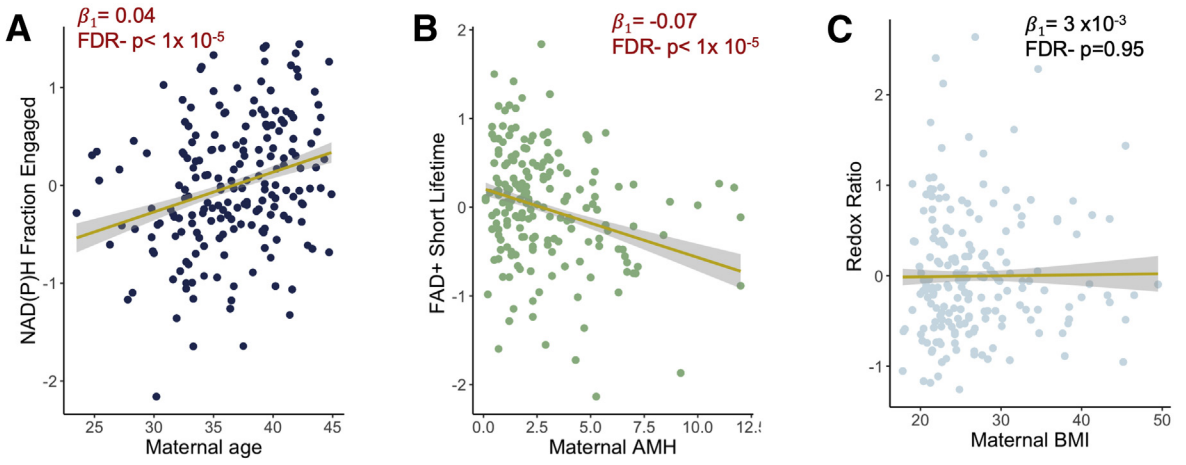

D

$$FLIMparam_{ijk} = \beta_0 + \beta_1 * Patient\ Factor + c_k + b_{jk} + e_{ijk}$$

Patient Factor	NAD(P)H irradiance	NAD(P)H Fraction Engaged	NAD(P)H Long Lifetime	NAD(P)H Short Lifetime	FAD+ irradiance	FAD+ Fraction Engaged	FAD+ Long Lifetime	FAD+ Short Lifetime	Redox Ratio
Age	β_1= 0.03 FDR-p=5x10^{-3}	β_1 = 0.04 FDR-p<1x 10^{-5}	β_1= 0.04 FDR-p<1x 10^{-5}	β_1= 0.01 FDR-p=0.26	β_1= 0.02 FDR-p=0.08	β_1= -0.29 FDR-p=0.05	β_1= 0.02 FDR-p=0.15	β_1= 0.05 FDR-p<1x 10^{-5}	β_1= 0.02 FDR-p=0.15
AMH	β_1= -0.05 FDR-p=0.02	β_1= -0.08 FDR-p<1x 10^{-5}	β = -0.09 FDR-p<1x 10^{-5}	β_1= -0.04 FDR-p=0.03	β_1 = -0.05 FDR-p=3x 10^{-3}	β_1= 0.03 FDR-p=0.27	β_1= 1x10^{-4} FDR-p=1.0	β_1= -0.07 FDR-p<1x 10^{-5}	β_1 = -0.02 FDR-p=0.48
BMI	β_1= -4x10^{-3} FDR-p=0.95	β_1= 4x10^{-4} FDR-p=0.95	β_1= -9x10^{-4} FDR-p=0.95	β_1= 6x10^{-3} FDR-p=0.95	β_1= -6x10^{-3} FDR-p=0.95	β_1= 2x10^{-3} FDR-p=0.95	β_1= 4x10^{-3} FDR-p=0.95	β_1 = -7x10^{-3} FDR-p=0.95	β_1= 1x10^{-3} FDR-p=0.95
% Patient Variance explained by age and AMH	9%	20%	20%	2%	3%	11%	0%	33%	0.1%

Cumulus cell FLIM metabolic parameters are associated with patient clinically relevant factors. The normalized NAD(P)H fraction engaged is significantly associated with maternal age (**A**), the FAD+ short lifetime is significantly associated with maternal AMH level (**B**), and the redox ratio is not significantly associated with maternal BMI (**C**). Each dot corresponds to the mean for each patient. (**D**) A multilevel model was used to determine the significance (i.e., *P* value) and the extent of correlation (i.e., β_1-coefficient) of CC FLIM parameters with maternal age, BMI, and AMH level. Numbers in red are statistically significant after correcting for multiple comparisons using the Benjamini-Hochberg FDR *P* value <.05. The last row shows the percentage of the CC FLIM parameters variance between patients that is explained by both age and AMH level. AMH = antimüllerian hormone; BMI = body mass index; CC = cumulus cluster; FAD+ = flavine adenine dinucleotide; FDR = false discovery rate; FLIM = fluorescence lifetime imaging microscopy; NAD(P)H = nicotinamide adenine (phosphate) dinucleotide.

Venturas. Metabolic imaging of human cumulus cells. Fertil Steril 2021.

CCs affects oocyte growth and quality (37). The effects of CC metabolic state on the corresponding oocyte have attracted much attention in recent years. In view of the importance of CC mitochondrial function for successful oocyte developmental competence (14), CC metabolic state may act as a biologic marker of oocyte quality.

In this study, we used FLIM of NAD(P)H and FAD+ to quantitatively determine the metabolic state of CCs. Analysis of 8 to 10 FLIM images acquired throughout each of 619 CC clusters from 193 patients revealed that for all FLIM parameters, the variance associated with differences between CCs of different oocytes was larger than the variance associated with differences between patients and between individual images obtained from the same cluster. Additionally, we observed that CC metabolic parameters were associated with maternal clinical factors that are known to be key determinants of oocyte quality. Finally, we found significant differences in NAD(P)H FLIM parameters and redox ratio between CC clusters from mature and immature oocytes.

By analyzing our hierarchically organized data using multilevel modeling (33, 36), we obtained the variances in FLIM parameters within the three levels: variance associated

FIGURE 4

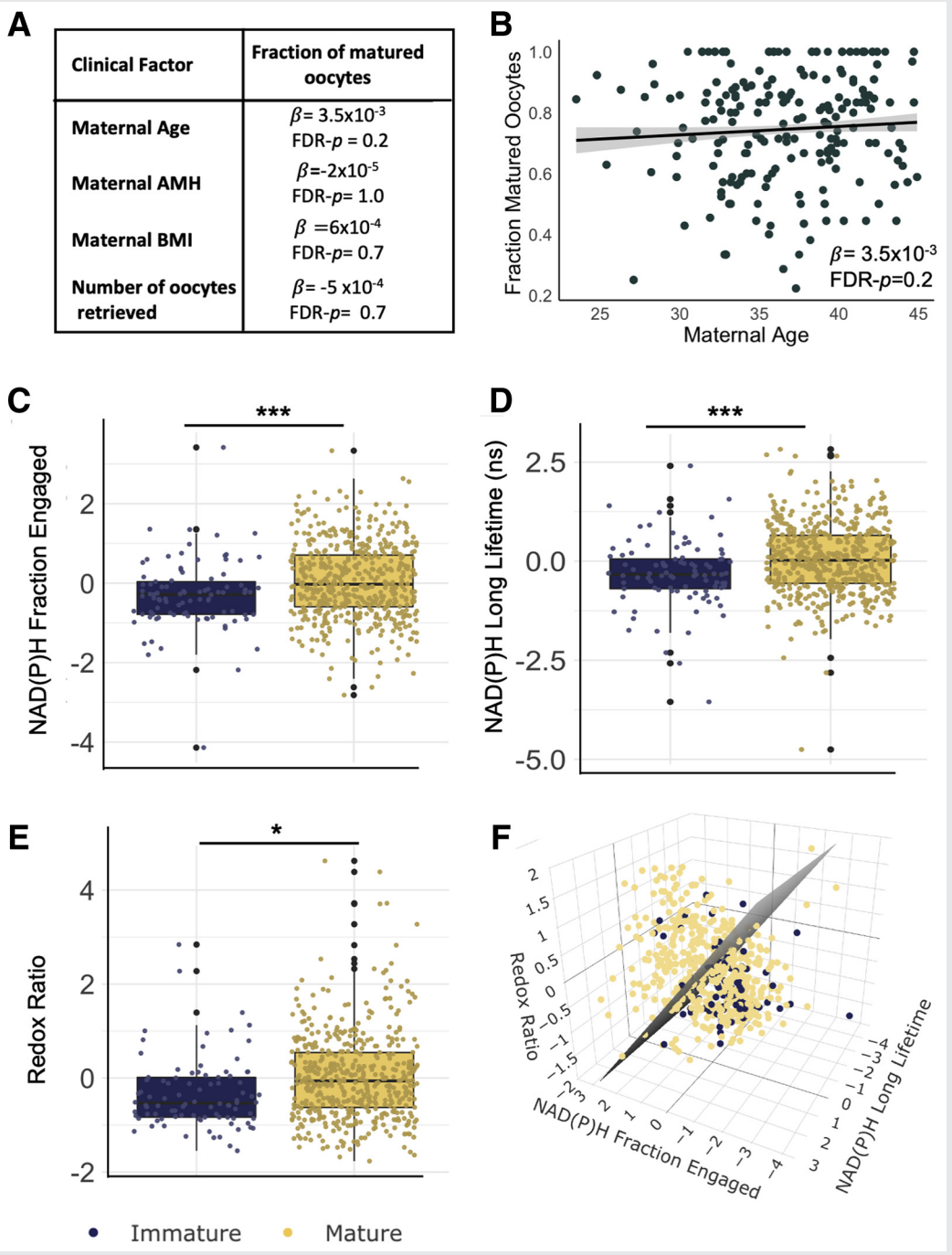

Cumulus cell FLIM metabolic parameters are associated with the maturity of the enclosed oocyte. (**A**) -Coefficients and FDR *P* values of the linear regression of maternal age, BMI, AMH level, and number of oocytes retrieved with the fraction of matured oocytes (number of matured oocytes/ total number of oocytes retrieved). There are no significant associations between these patient clinical factors and the fraction of matured oocytes.(**B**) Fraction of matured oocytes plotted vs. maternal age indicates no significant association. However, significant differences were found between CCs of immature (n = 90, blue) and mature (n = 505, yellow) oocytes in normalized NAD(P)H irradiance, NAD(P)H fraction bound (**C**), NAD(P)H long lifetime (**D**), and redox ratio (**E**). (**F**) Three-dimensional plot of these three FLIM parameters for each CC cluster. In gray, support vector machine was applied to draw a hyperplane that best separates the two groups. *FDR $P<.05$, *** FDR $P<.001$. AMH = antimüllerian hormone; BMI = body mass index; CC = cumulus cluster; FDR = false discovery rate; FLIM = fluorescence lifetime imaging microscopy; NAD(P)H = nicotinamide adenine (phosphate) dinucleotide.

Venturas. Metabolic imaging of human cumulus cells. Fertil Steril 2021.

with differences between patients, variance associated with differences between CC clusters from the same patient, and variance associated with differences between individual images from the same cluster. We found a large variance in all FLIM metabolic parameters between CC clusters, indicating that CCs associated with individual oocytes from the same patient have significantly different metabolic states.

The fact that there are measurable differences between CCs associated with individual oocytes highlights the potential use of this approach to determine oocyte-specific characteristics. Additionally, the small variance in FLIM parameters associated with the differences between images of the same CC cluster indicates the high reproducibility of these measurements. However, this variance was not null, which might be due either to minor errors in the FLIM measurements or to a true heterogeneity of metabolic state within a CC cluster. The latter is unlikely, since our validation studies showed only minor deviations in FLIM measurements among samples from the same cumulus cluster. The variance in FLIM parameters associated with differences between patients indicates that patient-specific factors impact the metabolism of their CCs. Patient-specific effects on CC mtDNA measurements have been previously reported (18).

Patient factors, such as age, BMI, and measures of ovarian reserve, such as AMH, have long been associated with oocyte quality (38, 39). We found significant associations between CC metabolic state, as measured by FLIM of NAD(P)H and FAD+, and maternal age. The influence of maternal age on CC metabolism has been demonstrated in several studies (21, 40–42). Both proteomic and genomic analyses of CCs in women of advanced age differ from those in younger women (40, 41). Cumulus cells from older woman have been shown to contain higher numbers of damaged mitochondria and mtDNA alterations (42, 43). In addition, we observed a significant association between CC FLIM parameters and AMH level, even after controlling for maternal age. This observation is consistent with previous results that found a correlation between CC mitochondrial membrane potential and measures of ovarian reserve (13). The levels of gonadotropins administered were significantly correlated with several FLIM parameters. Since these associations depend on both maternal age and AMH level, they are unlikely to be caused by direct interactions. Future studies will be required to clarify the interplay between patient-specific factors that impact CC FLIM parameters.

Our results did not indicate an association between CC metabolic state and maternal BMI. This contrasts with a study by Gorshinova et al. (27), which found a reduction in active mitochondria with increasing maternal BMI in a group of 13 patients. However, only a small portion of the patient-level variance in FLIM parameters can be explained by age and AMH level. This argues that CC metabolic state is also influenced by other patient-specific factors, such as metabolic diseases, genetic predisposition, diet, and smoking. Future studies will disentangle the effects of these additional factors. In mitochondria of mouse oocytes, a simultaneous increase in NAD(P)H intensity and fraction engaged corresponded to an increase in metabolic flux through the electron transport chain (44). If the same held for human CCs, it would imply that mitochondrial metabolic fluxes in CCs increase with patient age and decrease with ovarian reserve. However, this conclusion must be treated with caution because of the extensive metabolic differences between CCs and oocytes. Additional experiments will be necessary to definitively determine the biologic basis of the trends in FLIM parameters in CCs that we observed in this study.

CC-oocyte crosstalk is a key determinant for acquisition of oocyte developmental competence and CC maturation (4, 8, 11, 12). Oocyte quality depends on successful nuclear and cytoplasmic maturation (7, 10) as well as maternal clinical factors (38, 39). The results of our study indicated that the fraction of mature oocytes at retrieval was not correlated with any patient clinical characteristics, such as age, BMI, or AMH level, or even the number of oocytes retrieved. However, variations in FLIM metabolic parameters were observed between CC clusters associated with mature oocytes and those associated with immature oocytes. Cumulus cell and oocyte metabolic communication is essential not only for the resumption of meiosis (1, 11), but also for the acquisition of developmental competence (8, 12). Interestingly, we found that CCs from mature oocytes had a higher NAD(P)H fraction bound, NAD(P)H long lifetime, and redox ratio (NAD(P)H intensity: FAD+ intensity) than CCs from immature oocytes. These findings are in line with previous studies demonstrating a low mitochondrial membrane potential in CCs from immature oocytes compared with those from mature oocytes (13), as well as those with differences in mtDNA copy number (14, 15). We therefore conclude that FLIM imaging can detect metabolic variations in cumulus masses from immature oocytes compared with mature oocytes. However, we also observed large variations in FLIM parameters across CC clusters from mature oocytes and large variations in FLIM parameters across CCs from immature oocytes. These findings highlight the difficulty of developing a prediction model to assess oocyte maturity.

CONCLUSION

In summary, metabolic imaging of human CCs by FLIM is a promising approach for detecting variations in metabolic state of these cells. Fluorescence lifetime imaging microscopy sensitively detects variations in CC metabolism and shows a greater variance in FLIM parameters among oocytes than between patients. Cumulus cell metabolic parameters are associated with clinically relevant factors such as age and AMH level, but not with BMI. Moreover, metabolic imaging detects significant differences between the CC metabolic state of immature and mature oocytes. A greater understanding of the metabolic underpinnings of human CC-oocyte interactions could offer new opportunities for improving fertility interventions, in particular in vitro maturation protocols.

Acknowledgments: The authors thank Becker and Hickl for contributing a single-photon-counting detector and TCSPC electronics to this study. The authors also thank Brian Leahy,

Ph.D., for useful advice, as well as all members of the embryology team at Brigham and Women's Hospital for their assistance in the collection of the cumulus samples for this research. Images were created with BioRender.com

DIALOG: You can discuss this article with its authors and other readers at https://www.fertstertdialog.com/posts/32893

REFERENCES

1. Eppig JJ. Intercommunication between mammalian oocytes and companion somatic cells. Bioessays 1991;13:569–74.
2. Albertini DF, Combelles CM, Benecchi E, Carabatsos MJ. Cellular basis for paracrine regulation of ovarian follicle development. Reproduction 2001;121:647–53.
3. Anderson E, Albertini DF. Gap junctions between the oocyte and companion follicle cells in the mammalian ovary. J Cell Biol 1976;71:680–6.
4. Eppig JJ. Oocyte control of ovarian follicular development and function in mammals. Reproduction 2001;122:829–38.
5. Seli E, Babayev E, Collins SC, Nemeth G, Horvath TL. Minireview: metabolism of female reproduction: regulatory mechanisms and clinical implications. Mol Endocrinol 2014;28:790–804.
6. Dumesic DA, Meldrum DR, Katz-Jaffe MG, Krisher RL, Schoolcraft WB. Oocyte environment: follicular fluid and cumulus cells are critical for oocyte health. Fertil Steril 2015;103:303–16.
7. Keefe D, Kumar M, Kalmbach K. Oocyte competency is the key to embryo potential. Fertil Steril 2015;103:317–22.
8. Sutton ML, Cetica PD, Beconi MT, Kind KL, Gilchrist RB, Thompson JG. Influence of oocyte-secreted factors and culture duration on the metabolic activity of bovine cumulus cell complexes. Reproduction 2003;126:27–34.
9. Gilchrist RB, Lane M, Thompson JG. Oocyte-secreted factors: regulators of cumulus cell function and oocyte quality. Hum Reprod Update 2008;14:159–77.
10. Watson AJ. Oocyte cytoplasmic maturation: a key mediator of oocyte and embryo developmental competence. J Anim Sci 2007;85:E1–3.
11. Fagbohun CF, Downs SM. Metabolic coupling and ligand-stimulated meiotic maturation in the mouse oocyte-cumulus cell complex1. Biol Reprod 1991;45:851–9.
12. Downs SM, Humpherson PG, Leese HJ. Pyruvate utilization by mouse oocytes is influenced by meiotic status and the cumulus oophorus. Mol Reprod Dev 2002;62:113–23.
13. Anderson SH, Glassner MJ, Melnikov A, Friedman G, Orynbayeva Z. Respirometric reserve capacity of cumulus cell mitochondria correlates with oocyte maturity. J Assist Reprod Genet 2018;35:1821–30.
14. Boucret L, Bris C, Seegers V, Goudenège D, Desquiret-Dumas V, Domin-Bernhard M, et al. Deep sequencing shows that oocytes are not prone to accumulate mtDNA heteroplasmic mutations during ovarian ageing. Hum Reprod 2017;32:2101–9.
15. Lan Y, Zhang S, Gong F, Lu C, Lin G, Hu L. The mitochondrial DNA copy number of cumulus granulosa cells may be related to the maturity of oocyte cytoplasm. Hum Reprod 2020;35:1120–9.
16. Fontana J, Martínková S, Petr J, Žalmanová T, Trnka J. Metabolic cooperation in the ovarian follicle. Physiol Res 2020;69:33–48.
17. Ogino M, Tsubamoto H, Sakata K, Oohama N, Hayakawa H, Kojima T, et al. Mitochondrial DNA copy number in cumulus cells is a strong predictor of obtaining good-quality embryos after IVF. J Assist Reprod Genet 2016;33:367–71.
18. Desquiret-Dumas V, Clément A, Seegers V, Boucret L, Ferré-L'Hotellier V, Bouet PE, et al. The mitochondrial DNA content of cumulus granulosa cells is linked to embryo quality. Hum Reprod 2017;32:607–14.
19. Cinco R, Digman MA, Gratton E, Luderer U. Spatial characterization of bioenergetics and metabolism of primordial to preovulatory follicles in whole ex vivo murine ovary. Biol Reprod 2016;95:129.
20. Assou S, Haouzi D, Mahmoud K, Aouacheria A, Guillemin Y, Pantesco V, et al. A non-invasive test for assessing embryo potential by gene expression profiles of human cumulus cells: a proof of concept study. Mol Hum Reprod 2008;14:711–9.
21. Boucret L, Chao de la Barca JM, Morinière C, Desquiret V, Ferré-L'Hôtellier V, Descamps P, et al. Relationship between diminished ovarian reserve and mitochondrial biogenesis in cumulus cells. Hum Reprod 2015;30:1653–64.
22. Gebhardt KM, Feil DK, Dunning KR, Lane M, Russell DL. Human cumulus cell gene expression as a biomarker of pregnancy outcome after single embryo transfer. Fertil Steril 2011;96:47–52.e2.
23. Huang Z, Wells D. The human oocyte and cumulus cells relationship: new insights from the cumulus cell transcriptome. Mol Hum Reprod 2010;16:715–25.
24. McKenzie LJ, Pangas SA, Carson SA, Kovanci E, Cisneros P, Buster JE, et al. Human cumulus granulosa cell gene expression: a predictor of fertilization and embryo selection in women undergoing IVF. Hum Reprod 2004;19:2869–74.
25. Uyar A, Torrealday S, Seli E. Cumulus and granulosa cell markers of oocyte and embryo quality. Fertil Steril 2013;99:979–97.
26. Taugourdeau A, Desquiret-Dumas V, Hamel JF, Chupin S, Boucret L, Ferré-L'Hotellier V, et al. The mitochondrial DNA content of cumulus cells may help predict embryo implantation. J Assist Reprod Genet 2019;36:223–8.
27. Gorshinova VK, Tsvirkun DV, Sukhanova IA, Tarasova NV, Volodina MA, Marey MV, et al. Cumulus cell mitochondrial activity in relation to body mass index in women undergoing assisted reproductive therapy. BBA Clin 2017;7:141–6.
28. Heikal AA. Intracellular coenzymes as natural biomarkers for metabolic activities and mitochondrial anomalies. Biomark Med 2010;4:241–63.
29. Dumollard R, Marangos P, Fitzharris G, Swann K, Duchen M, Carroll J. Sperm-triggered [Ca2+] oscillations and Ca2+ homeostasis in the mouse egg have an absolute requirement for mitochondrial ATP production. Development 2004;131:3057–67.
30. Klaidman LK, Leung AC, Adams JD. High-performance liquid chromatography analysis of oxidized and reduced pyridine dinucleotides in specific brain regions. Anal Biochem 1995;228:312–7.
31. Ghukasyan VV, Heikal AA, editors. Natural Biomarkers for Cellular Metabolism: Biology, Techniques, and Applications. Boca Raton: CRC Press; 2014.
32. Becker W. Fluorescence lifetime imaging—techniques and applications. J Microsc 2012;247:119–36.
33. Snijders TAB, Bosker RJ. Multilevel Analysis: an Introduction to Basic and Advanced Multilevel Modeling. Thousand Oaks: SAGE; 2011.
34. Stein LR, Imai S. The dynamic regulation of NAD metabolism in mitochondria. Trends Endocrinol Metab 2012;23:420–8.
35. Berg S, Kutra D, Kroeger T, Straehle CN, Kausler BX, Haubold C, et al. Ilastik: interactive machine learning for (bio)image analysis. Nat Methods 2019;16:1226–32.
36. Lorah J. Effect size measures for multilevel models: definition, interpretation, and TIMSS example. Large Scale Assess Educ 2018;6:8.
37. Dumesic DA, Guedikian AA, Madrigal VK, Phan JD, Hill DL, Alvarez JP, et al. Cumulus cell mitochondrial resistance to stress in vitro predicts oocyte development during assisted reproduction. J Clin Endocrinol Metab 2016;101:2235–45.
38. Cimadomo D, Fabozzi G, Vaiarelli A, Ubaldi N, Ubaldi FM, Rienzi L. Impact of maternal age on oocyte and embryo competence. Front Endocrinol (Lausanne) [Internet] 2018;9. Available at: https://www.ncbi.nlm.nih.gov/pmc/articles/PMC6033961/. Accessed March 26, 2021.
39. Zhang J-J, Liu X, Chen L, Zhang S, Zhang X, Hao C, et al. Advanced maternal age alters expression of maternal effect genes that are essential for human oocyte quality. Aging (Albany NY) 2020;12:3950–61.
40. May-Panloup P, Boucret L, Chao de la Barca J-M, Desquiret-Dumas V, Ferré-L'Hotellier V, Morinière C, et al. Ovarian ageing: the role of mitochondria in oocytes and follicles. Hum Reprod Update 2016;22:725–43.
41. McReynolds S, Dzieciatkowska M, McCallie BR, Mitchell SD, Stevens J, Hansen K, et al. Impact of maternal aging on the molecular signature of human cumulus cells. Fertil Steril 2012;98:1574–80.e5.
42. Tatone C, Carbone MC, Falone S, Aimola P, Giardinelli A, Caserta D, et al. Age-dependent changes in the expression of superoxide dismutases and

catalase are associated with ultrastructural modifications in human granulosa cells. Mol Hum Reprod 2006;12:655–60.

43. Seifer DB, DeJesus V, Hubbard K. Mitochondrial deletions in luteinized granulosa cells as a function of age in women undergoing in vitro fertilization. Fertil Steril 2002;78:1046–8.

44. Yang X, Needleman DJ. Coarse-grained model of mitochondrial metabolism enables subcellular flux inference from fluorescence lifetime imaging of NADH [Internet]. Biophysics; 2020. Available at: http://biorxiv.org/lookup/doi/10.1101/2020.11.20.392225. Accessed April 13, 2021.